The BBSome in POMC and AgRP Neurons Is Necessary for Body Weight Regulation and Sorting of Metabolic Receptors

Deng-Fu Guo,[1] Zhihong Lin,[1] Yuanming Wu,[2] Charles Searby,[3] Daniel R. Thedens,[4] George B. Richerson,[2] Yuriy M. Usachev,[1,5] Justin L. Grobe,[1,5,6] Val C. Sheffield,[3,5,6] and Kamal Rahmouni[1,5,6,7]

Diabetes 2019;68:1591–1603 | https://doi.org/10.2337/db18-1088

The BBSome, a complex of eight Bardet-Biedl syndrome (BBS) proteins involved in cilia function, has emerged as an important regulator of energy balance, but the underlying cellular and molecular mechanisms are not fully understood. Here, we show that the control of energy homeostasis by the anorexigenic proopiomelanocortin (POMC) neurons and orexigenic agouti-related peptide (AgRP) neurons require intact BBSome. Targeted disruption of the BBSome by *Bbs1* gene deletion in POMC or AgRP neurons increases body weight and adiposity. We demonstrate that obesity in mice lacking the *Bbs1* gene in POMC neurons is associated with hyperphagia. Mechanistically, we present evidence implicating the BBSome in the trafficking of G protein–coupled neuropeptide Y Y2 receptor (NPY_2R) and serotonin 5-hydroxytryptamine ($HT)_{2C}$ receptor ($5\text{-}HT_{2C}R$) to cilia and plasma membrane, respectively. Consistent with this, loss of the BBSome reduced cell surface expression of the $5\text{-}HT_{2C}R$, interfered with serotonin-evoked increase in intracellular calcium and membrane potential, and blunted the anorectic and weight-reducing responses evoked by the $5\text{-}HT_{2C}R$ agonist, lorcaserin. Finally, we show that disruption of the BBSome causes the $5\text{-}HT_{2C}R$ to be stalled in the late endosome. Our results demonstrate the significance of the hypothalamic BBSome for the control of energy balance through regulation of trafficking of important metabolic receptors.

Genetic studies have consistently pointed to the central nervous system as a key player in the regulation of body weight and the development of obesity and its adverse side effects (1,2). This is consistent with the tremendous influence the brain exerts on the processes that control food intake and energy expenditure (3,4). The brain receives afferent signals about the status of body energy reserves, leading to autonomic, humoral, and behavioral adaptations aimed at maintaining body weight and adiposity in a normal range. These neuroendocrine systems are tightly controlled, and their disruption leads to obesity.

The distribution and mechanism of action of the key signals that influence metabolic functions point to a significant role of the hypothalamus in integrating the external and internal signals and in enacting appropriate and consequential metabolic and behavioral responses to maintain energy balance (3,4). Anorexigenic neurons expressing proopiomelanocortin (POMC) and orexigenic neurons expressing agouti-related peptide (AgRP) located in the hypothalamic arcuate nucleus are critically involved in the control of feeding and energy expenditure. These neurons are considered as first-order neurons that mediate the effects of various signals such as leptin, insulin, and serotonin (3,5–7). Despite being the most extensively studied neuronal populations regarding energy balance, our understanding of the molecular processes controlling their activity remains incomplete.

The BBSome is a complex composed of eight Bardet-Biedl syndrome (BBS) proteins (BBS1, BBS2, BBS4, BBS5, BBS7, BBS8, BBS9, and BBS18) (8,9). The assembly of the BBSome depends on another protein complex that contains three BBS proteins (BBS6, BBS10, and BBS12) (10,11).

[1]Department of Pharmacology, University of Iowa, Iowa City, IA
[2]Department of Neurology, University of Iowa, Iowa City, IA
[3]Department of Pediatrics, University of Iowa, Iowa City, IA
[4]Department of Radiology, University of Iowa, Iowa City, IA
[5]Fraternal Order of Eagles Diabetes Research Center, University of Iowa, Iowa City, IA
[6]Obesity Education and Research Initiative, University of Iowa, Iowa City, IA
[7]Department of Internal Medicine, University of Iowa, Iowa City, IA

Corresponding author: Kamal Rahmouni, kamal-rahmouni@uiowa.edu

Received 8 October 2018 and accepted 12 May 2019

This article contains Supplementary Data online at http://diabetes.diabetesjournals.org/lookup/suppl/doi:10.2337/db18-1088/-/DC1.

The discovery that various BBS proteins interact to form complexes that are critical is consistent with the overlapping phenotypes arising from mutations in different *BBS* genes (11). Indeed, mutation in *BBS* genes results in human diseases with multiple features, including obesity. In addition, variants of several *BBS* genes were found to increase susceptibility to obesity in individuals without BBS (12–14). Together, these findings highlight the importance of the BBSome for energy balance and the development of obesity, but the underlying mechanisms are not well understood.

The BBSome is a critical regulator of cilia function by targeting cargos to the ciliary membrane. Primary cilia are important signaling organelles present in virtually every cell type in the body, including neurons (15). A number of G protein–coupled receptors, including somatostatin receptor 3 ($SSTR_3$) (16), neuropeptide Y Y2 receptor (NPY_2R) (17), and melanocortin 4 receptor, localize to cilia (18). In addition to its involvement in the trafficking of cargos to cilia, the BBSome has emerged as a key mediator of many cellular processes, including the delivery of receptors to the plasma membrane (19,20).

Here, we reveal an important role of the BBSome in the control of energy balance by POMC and AgRP neurons. We show that selective disruption the BBSome, through *Bbs1* gene deletion in POMC or AgRP neurons, led to a significant increase in body weight and adiposity. We also uncover a critical role of the BBSome in the cellular trafficking of serotonin 5-hydroxytryptamine $(HT)_{2C}$ receptor ($5\text{-}HT_{2C}R$), an important receptor for energy homeostasis and the target of the antiobesity drug lorcaserin. Our data demonstrate that the BBSome is required for $5\text{-}HT_{2C}R$ trafficking to the plasma membrane, providing a molecular explanation for the obesity phenotype evoked by disruption of the BBSome.

RESEARCH DESIGN AND METHODS

Animals

All animal testing was approved by the University of Iowa Animal Care and Use Committee. Mice were housed in groups of three to five per cage and maintained on a 12-h light-dark cycle, with lights on at 6:00 A.M. Room temperature was maintained at 22°C. Food and water were available ad libitum.

To obtain selective deletion of the *Bbs1* gene in POMC or AgRP neurons, male transgenic $POMC^{Cre}$ or $AgRP^{Cre}$ mice (stock #005965 and 012899, respectively; The Jackson Laboratory) were crossed with $Bbs1^{fl/fl}$ female mice (20). $POMC^{Cre}/Bbs1^{fl/wt}$ and $AgRP^{Cre}/Bbs1^{fl/wt}$ offspring were subsequently crossed with $Bbs1^{fl/wt}$ mice to generate $POMC^{Cre}/Bbs1^{fl/fl}$ and $AgRP^{Cre}/Bbs1^{fl/fl}$ mice, respectively. The genotype of mice was determined by PCR analysis of tail DNA (20) using the primer sequences provided in Supplementary Table 1. A group of diet-induced obese C57BL/6J mice fed a high-fat diet (D12492; Research Diets) for 12 weeks and controls fed normal chow were obtained from The Jackson Laboratory.

Metabolic Studies

Mice were weighed once weekly, beginning at weaning (4 weeks of age) until 25 weeks of age. Body composition was determined by MRI under anesthesia (91 mg/kg ketamine and 9.1 mg/kg xylazine, i.p.) using a Varian Unity/Inova 4.7 T small-bore MRI system (Varian). To measure food intake, mice were housed individually in regular cages and allowed to acclimate for at least 3 days before measurements of 24-h food intake for 5 days. Resting metabolic rate was measured by push-pull respirometry at thermoneutrality during the daytime, as described previously (20).

Food intake and body weight response to lorcaserin were compared between control animals, $POMC^{Cre}/Bbs1^{fl/fl}$ mice, and diet-induced obese mice. Baseline body weight and food intake of individually housed mice were measured daily for 5 consecutive days before beginning treatment with vehicle or lorcaserin (1 μg/μL/g body wt i.p., twice daily at 8:00 A.M. and 5:00 P.M., for 4 days).

Glucose and Insulin Tolerance Tests and Insulin Measurements

Glucose tolerance tests (GTTs) and insulin tolerance tests (ITTs) were performed as described previously. Mice were fasted overnight (GTT) or for 5 h (ITT) in a clean cage. Basal blood glucose measurements were taken before injection of glucose (2 g/kg i.p.) or insulin (1 unit/kg i.p.). Blood glucose measurements were assessed multiple times during the 2-h test. Plasma insulin levels were measured using an ELISA kit (RayBiotech).

Generation of the Mouse IMCD3 *Bbs1* Knockout Cell Line

The human codon-optimized Cas9 plasmid pX459 (#48139) was obtained from Addgene. Single guide (sg)RNAs were designed and constructed as described previously. Briefly, target 20 base pair (bp) sequences starting with guanine and preceding the protospacer adjacent motif (5′-NGG-3′) were selected from the mouse *Bbs1* exon 4. Potential off-target effects of sgRNA candidates were analyzed using the online tool CRISPR Design (http://crispr.mit.edu/). One sgRNA in exon 4 (Supplementary Table 1) of the mouse *Bbs1* gene was selected for transfection to create knockout cell lines. Clonal genomic DNA was extracted and used for PCR and Sanger sequencing with the forward primer and the reverse primer (Supplementary Table 1). This resulted in cell lines with homozygous 1 bp T insertions and homozygous 2 bp deletions (cytosine and thymine) in exon 4.

Mouse kidney epithelial cells (mIMCC-3; #CRL-2123, ATCC) were cultured in DMEM/F12 (Life Technologies) supplemented with 10% FCS. Cells were seeded in a 6-well plate at 1×10^6 cells/well. Transfection was performed with Lipofectamine 2000 using recommended conditions. Briefly, 2 μg plasmid containing an sgRNA targeting *Bbs1* exon 4 and 6 μL Lipofectamine 2000 were diluted in 100 μL Opti-MEM, mixed 1:1, and added to cells after 5 min of incubation. After 24 h, the cells were passed at low

density (2,000 cells/well) in 10-cm culture dishes and selected with puromycin at 1.5 μg/mL for clonal expansion. The media were changed every 2 days until colonies were harvested using cloning cylinders.

Measurement of Intracellular Ca^{2+}

IMCD3 and IMCD3-*Bbs1*$^{-/-}$ cells were transiently transfected with 5-HT_{2C}R tagged with green fluorescent protein (GFP). The cells were loaded with fura-2 48 h after transfection using the acetoxymethyl ester form of the indicator (fura-2/AM) (2 μmol/L for 30 min) to monitor changes in the intracellular Ca^{2+} concentration ($[Ca^{2+}]_i$) in response to 5 μmol/L serotonin and then to 10 μmol/L ATP. The cells were placed in a chamber for flow-through perfusion, mounted on an inverted IX-71 microscope (Olympus), and perfused with HEPES-buffered Hanks' balanced salt solution composed of 140 mmol/L NaCl, 5 mmol/L KCl, 1.3 mmol/L $CaCl_2$, 0.4 mmol/L $MgSO_4$, 0.5 mmol/L $MgCl_2$, 0.4 mmol/L KH_2PO_4, 0.6 mmol/L $NaHPO_4$, 3 mmol/L $NaHCO_3$, 10 mmol/L glucose, and 10 mmol/L HEPES, pH 7.4, with NaOH (310 mOsm/kg with sucrose).

Fluorescence was excited sequentially at 340 nm (12-nm bandpass) and 380 nm (12-nm bandpass) by using a Polychrome V monochromator (TILL Photonics) and focused on the cells via a 20×, 0.75 numerical aperture objective (Olympus). Fluorescence emission was measured at 540 nm (50-nm bandpass) using an IMAGO charge-coupled device camera (640 × 480 pixels; TILL Photonics). Two-by-two binning was used for acquisition (1 pixel, ~500 nm). A series of 340-nm and 380-nm images was acquired every 2 s. ATP (10 μmol/L) was also used as a positive control. $[Ca^{2+}]_i$ data were analyzed using TILLvisION (TILL Photonics) software and presented as F_{340}-to-F_{380} ratio, where F_{340} and F_{380} correspond to the fluorescence intensity at excitation wavelength 340 and 380 nm, respectively. The F_{340} and F_{380} values were corrected for background, which was determined for each experiment by measuring fluorescence at 340 and 380 nm in an area free of cells.

Electrophysiological Recording

HEK 293 cells were used to measure serotonin-induced membrane potential. Briefly, the cells were cotransfected with control shRNA or *Bbs1*-shRNA with GFP-tagged 5-HT_{2c}R. At 72 h after transfection, cells were placed in a perfusion chamber mounted on the stage of an upright Zeiss Axioskop FS2 microscope (Carl Zeiss) equipped with a Hamamatsu C2741-60 charged-coupled device camera (Hamamatsu Photonics). Epifluorescence was briefly used to target fluorescent cells, after which the light source was switched to infrared differential interference contrast imaging to allow visualization while obtaining whole-cell patch clamp recordings. Membrane potentials were recorded in current clamp mode using an Axopatch 700B amplifier (Molecular Devices), low-pass filtered at 1 kHz, digitized at 10 kHz, and analyzed offline on a personal computer with pCLAMP (Molecular Devices) and Origin software (OriginLab). Recording electrodes had resistances of 2.5–5 MΩ when filled with the K-gluconate pipette solution, which contained 120 mmol/L K-gluconate, 10 mmol/L KCl, 10 mmol/L HEPES, 5 mmol/L EGTA, 1 mmol/L $CaCl_2$, 1 mmol/L $MgCl_2$, and 5 mmol/L Mg-ATP adjusted to pH 7.3.

Biochemical Analysis

To detect cell surface receptor expression, cell surface biotinylation assays were performed in HEK 293 cells transiently transfected with the pcDNA3-Flag-5-HT_{2C}R receptor (Flag-5-HT_{2C}R), with *Bbs2*-shRNA or control shRNA on an LKO1 plasmid with X-tremeGENE 9 transfection reagent (Roche). Silencing efficacy of *Bbs2*-shRNA was reported previously (20).

The cells were incubated 48 h after transfection with cleavable EZ-Link Sulfo-NHS-SS-Biotin (Thermo Scientific) for 30 min on ice, and biotinylated proteins were recovered by using streptavidin-agarose beads (GE Healthcare). Beads were resuspended in Laemmli buffer, and bound proteins were separated by SDS-PAGE and detected by immunoblotting using mouse M2 anti-Flag (F1804; Sigma-Aldrich) to detect 5-HT_{2C}R and mouse anti-transferrin receptor (Invitrogen) monoclonal antibody.

To detect interaction between BBS1 or other BBSome proteins and CD63, HEK 293 cells were transiently transfected with hemagglutinin (HA)-tagged BBS1, BBS2, BBS4, BBS5, BBS7, BBS8, or BBS9 plasmids with control shRNA or *Bbs2*-shRNA. The cells were lysed 48 h after transfection with lysate buffer (50 mmol/L HEPES, pH 7.5, 150 mmol/L NaCl, 1 mmol/L $MgCl_2$, 1 mmol/L $CaCl_2$, 10 mmol/L NaF, 5 mmol/L EDTA, 1% Triton, 2 mmol/L sodium orthovanadate, and Roche cocktail protease inhibitor tablet). Cellular protein samples (800 μg) were subjected to immunoprecipitation assay with 5 μg anti-HA antibody (11815016001; Roche Applied Science). Immunocomplex was separated on a 9% SDS-PAGE gel, transferred to polyvinylidene fluoride membrane, and probed with anti-CD63 antibody (1:1,000) (EXOAB-CD63A-1; SBI System Biosciences), followed by a secondary anti-rabbit horse radish peroxidase goat antibody (1:10,000) (7074; Cell Signaling) or a goat anti-mouse horseradish peroxidase (1:10,000) (7076; Cell Signaling). Protein expression was visualized with the ECL detection kit (GE Healthcare) and exposed to film.

Gene Expression Analysis

Mice were sacrificed by CO_2 asphyxiation, and the brain was quickly isolated and put on ice. The mediobasal hypothalamus was carefully dissected and total RNA isolated using the RNeasy Plus Mini Kit (Qiagen). Total RNA (2 μg in final volume of 40 μL) was used to synthesize first-strand cDNAs with the Super-Script preamplification system. Then, 10 μL cDNA and 0.4 mmol/L primers were added in a final volume of 25 μL PCR mixture (iQ SYBR Green supermix, Bio-Rad) and amplified in a iQ5 Multicolor Real-Time PCR Detection System (Bio-Rad). The PCR

conditions for all genes were as follows: denaturation for 5 min at 95°C, 40 cycles for 30 s at 95°C, and 30 s at 60°C. S18 rRNA expression was used as internal control to normalize mRNA expression of these genes. Primer sequences are provided in Supplementary Table 1.

RNAscope

To detect Bbs1 and POMC mRNA, the brain was freshly harvested and put into optimum cutting temperature solution. The brain was sectioned with a cryostat, and the brain sections were hybridized with specific probes purchased from Advanced Cell Diagnostics (491121 for *Bbs1* and 314081-C2 for *POMC*). Processed brain sections were mounted using VectaShield mounting medium with DAPI. Images were visualized using confocal microscopy (LSM710; Zeiss) and analyzed using ImageJ software.

Immunofluorescence

Mice anesthetized with ketamine and xylazine were perfused with 50 mL PBS (5 mL/min), followed by 4% paraformaldehyde/HistoChoice Tissue Fixative (Amresco) in 50 mL PBS (2.5 mL/min) using a Harvard PHD 22/2000 Syringe Pump. The entire brain was excised and incubated in the same fixative overnight at 4°C. Fixed brains were washed three times with PBS and incubated in 30% sucrose/PBS overnight with one change of solution after 4–6 h of initial incubation. Brains were vibratome sectioned with 30-μm thickness. Immunochemistry was performed on brain sections using antibodies against POMC (1:250) (H-029-30; Phoenix Pharmaceuticals), phosphorylated Stat3 (1:1,000) (#9131S; Cell Signaling), 5-HT_{2C}R (1:250) (RA24505; Neuromics), NPY_2R (1:250) (14112; Neuromics), or adenylyl cyclase type III (1:250 dilution) (sc-32113 [N-14]; Santa Cruz Biotechnology), as described previously (20,21). For phosphorylated Stat3 staining, mice were fasted overnight and treated with leptin (2 mg/kg, i.p.) 1 h before sacrifice. The anti–5-HT_{2C}R antibody was validated using cells expressing a GFP-tagged 5-HT_{2C}R and brains of *5-$HT_{2C}R^{-/-}$* mice (provided by Dr. J. Elmquist, University of Texas Southwestern Medical Center). Processed brain sections were mounted using VectaShield mounting medium with DAPI. Images were visualized using confocal microscopy (LSM710; Zeiss) and analyzed using ImageJ software.

IMCD3 and IMCD3-*$Bbs1^{-/-}$* cells were transfected with GFP-tagged 5-HT_{2C}R, NPY_2R, or $SSTR_3$, and cilia were stained with acetylated α-tubulin (sc-23950; Santa Cruz Biotechnology). To detect 5-HT_{2C}R or BBS1 subcellular localization in IMCD3-*$Bbs1^{-/-}$* cells, the cells were transfected with GFP-tagged 5-HT_{2C}R or cotransfected with red fluorescent protein (RFP)-*Bbs1* with GFP-Rab5, GFP-Rab7, and GFP-Golgi, and then stained with early endosome marker EEA1 (3288; Cell Signaling), Lysosomal marker Lamp1 (9091; Cell Signaling), endosome marker Cav1 (3267; Cell Signaling), Golgi marker RCAS1 (12290; Cell Signaling), or late endosome marker CD63 (EXOAB-CD63A-1; SBI System Biosciences). HEK 293 cells were transiently cotransfected with GFP-tagged 5-HT_{2C}R with control shRNA or *Bbs2*-shRNA, and the receptor was visualized after 48 h of transfection.

Data Analysis

The data are expressed as means ± SEM and were analyzed using the Student *t* test or one- or two-way ANOVA. When ANOVA reached significance, a post hoc comparison was made using the Fisher test. A $P < 0.05$ value was considered statistically significant. Univariate regression modeling with body weight considered a covariate was used to assess resting metabolic rate data using SPSS software.

RESULTS

Selective Deletion of the *Bbs1* Gene in POMC Neurons Causes Obesity

In silico reanalysis of available single-cell RNA sequencing data sets from dissociated mouse hypothalamic cells (22) revealed that *BBS* genes are expressed in both POMC and AgRP neurons (Supplementary Fig. 1*A* and *B*). We have confirmed *Bbs1* gene expression in POMC neurons using RNAscope (Supplementary Fig. 1*C*). Strikingly, fasting was found to cause contrasting changes in the expression of several *BBS* genes in POMC versus AgRP neurons (Supplementary Fig. 1*A* and *B*). To determine the relevance of the BBSome in these neuronal populations for energy homeostasis, we generated mice bearing selective deletion of the *Bbs1* gene in POMC neurons ($POMC^{Cre}$/$Bbs1^{fl/fl}$ mice) by breeding the conditional $Bbs1^{fl/fl}$ mice with $POMC^{Cre}$ mice. Further crossing with a reporter mouse model expressing fluorescent td-Tomato (ROSA), in a Cre-dependent manner, confirmed the Cre-mediated recombination in POMC neurons (Supplementary Fig. 2*A* and *B*). It should be noted that absence of the BBS1 protein disrupts BBSome formation and function (20). Furthermore and consistent with previous reports implicating the BBSome in leptin sensitivity and leptin receptor (LepRb) trafficking (20,23), we found that leptin-induced Stat3 activation was blunted in td-$Tomato^{+}$ cells of the arcuate nucleus of $POMC^{cre}$/$Bbs1^{fl/fl}$ mice (Supplementary Fig. 2*C*).

Body weight was comparable between young (4–7 weeks old) $POMC^{Cre}$/$Bbs1^{fl/fl}$ mice and littermate controls (Fig. 1*A* and *B*). However, the body weight of both males and females begin to diverge at ∼8 weeks of age, with $POMC^{Cre}$/$Bbs1^{fl/fl}$ mice gaining more weight than the controls. The divergence in body weight continued over time, with $POMC^{Cre}$/$Bbs1^{fl/fl}$ mice weighing 10–17 g more than the control mice at 25 weeks of age (Fig. 1*A* and *B*). The increase in body weight in $POMC^{Cre}$/$Bbs1^{fl/fl}$ mice was due to an increase in adiposity, as indicated by the increased fat mass (Fig. 1*C* and *D* and Supplementary Fig. 2*D* and *E*). Liver mass was elevated in $POMC^{Cre}$/$Bbs1^{fl/fl}$ mice relative to controls (females: 1.74 ± 0.15 vs. 1.12 ± 0.09 g, $P < 0.05$; males: 2.94 ± 0.3 vs. 1.71 ± 0.08 g, $P < 0.05$). However, there was no difference in lean mass between $POMC^{Cre}$/$Bbs1^{fl/fl}$ mice and controls (Fig. 1*E*).

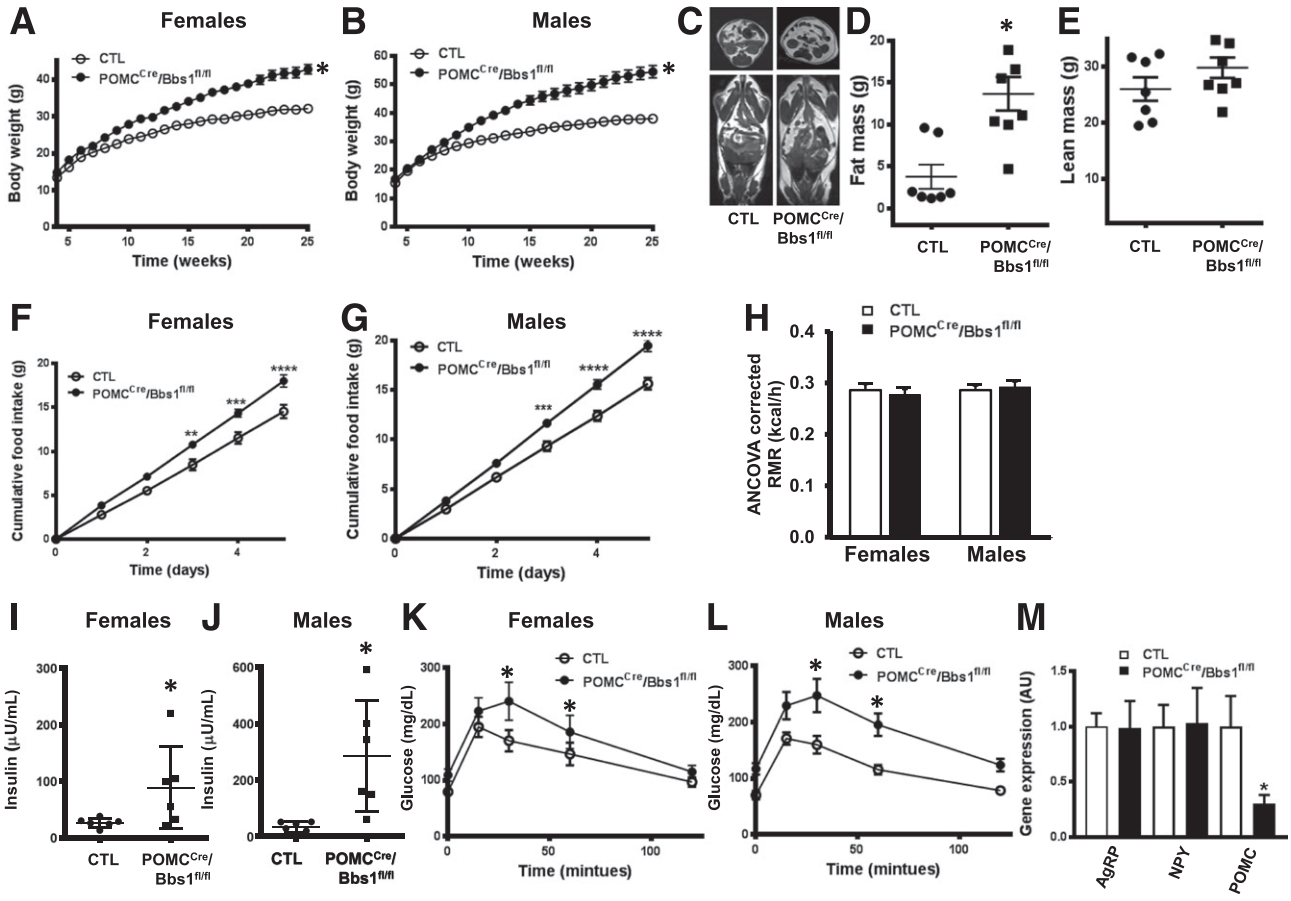

Figure 1—Mice lacking the *Bbs1* gene in POMC neurons develop obesity. Weekly body weights of female (*A*) and male (*B*) mice (n = 12–16/group: 12 males and 15 females for control [CTL] mice, 16 males and 16 females for POMC^{cre}/Bbs1$^{fl/fl}$ mice). *C–E*: Fat mass and lean mass, measured by MRI (n = 7/group: three males and four females in each group). *F* and *G*: Cumulative daily food intake (n = 6–13/group: 6 males and 12 females for control and 6 males and 13 females for POMC^{cre}/Bbs1$^{fl/fl}$ mice). *H*: Resting metabolic rate (RMR) (n = 4–6/group: six males and four females in each group), analyzed by univariate regression modeling (model, $P < 0.001$; body mass, $P < 0.001$; genotype, $P = 0.912$; sex, $P = 0.501$; interaction $P = 0.453$; body mass evaluated at 34.263 g; $R^2 = 0.772$). *I* and *J*: Plasma insulin levels. *K* and *L*: GTT (n = 10–12/group: 5 males and 5 females for controls and 6 males and 6 females for POMC^{cre}/Bbs1$^{fl/fl}$ mice). *M*: Hypothalamic mRNA levels of metabolic neuropeptides (n = 6/group: three males and three females in each group). *$P < 0.05$, **$P < 0.01$, ***$P < 0.001$, and ****$P < 0.0001$ vs. control group.

Consistent with the obesity phenotype, POMC^{Cre}/Bbs1$^{fl/fl}$ mice exhibited elevated food intake (Fig. 1*F* and *G*). In contrast, resting metabolic rate, corrected for body weight by univariate regression modeling (model $P < 0.001$, body weight $P < 0.001$), was comparable between POMC^{Cre}/Bbs1$^{fl/fl}$ mice and controls (Fig. 1*H*) (genotype $P = 0.912$, sex $P = 0.501$, interaction $P = 0.453$). These findings indicate that obesity in mice lacking the *Bbs1* gene in POMC neurons is driven by hyperphagia.

Circulating insulin levels were elevated in POMC^{Cre}/Bbs1$^{fl/fl}$ mice (Fig. 1*I* and *J*). A significant increase in fasting blood glucose was also noted in POMC^{Cre}/Bbs1$^{fl/fl}$ mice (114.7 ± 7.7 mg/dL) compared with controls (77.1 ± 6.8 mg/dL, $P < 0.05$). Moreover, POMC^{Cre}/Bbs1$^{fl/fl}$ mice displayed glucose intolerance (Fig. 1*K* and *L*) and tended to be insulin resistant (Supplementary Fig. 2*F* and *G*).

Interestingly, disruption of the BBSome in POMC neurons led to a significant decrease in the expression of the hypothalamic anorexigenic *Pomc* gene without altering the expression of orexigenic *Agrp* and *Npy* genes (Fig. 1*M*). Of note, there was no difference in the expression pattern of these genes between male and female POMC^{Cre}/Bbs1$^{fl/fl}$ mice. These findings highlight the relevance of the BBSome in POMC neurons for the mechanisms that underlie metabolic regulation.

Mice Lacking the *Bbs1* Gene in AgRP Neurons Are Obese

We previously reported that global BBS mice and mice lacking the *Bbs1* gene in the nervous system or LepRb-expressing cells have normal expression of hypothalamic *Agrp* and *Npy* genes. This led us to hypothesize that loss of the BBSome in AgRP neurons does not contribute to the obesity phenotype observed in these mice. To test this directly, we generated mice lacking the *Bbs1* gene selectively in AgRP neurons by breeding the Bbs1$^{fl/fl}$ mice with AgRP^{Cre} mice. As above, we used the td-Tomato (ROSA) reporter mouse model to confirm that AgRP^{Cre} drives Cre-recombinase, indicated by td-Tomato protein expression (Supplementary Fig. 3*A*).

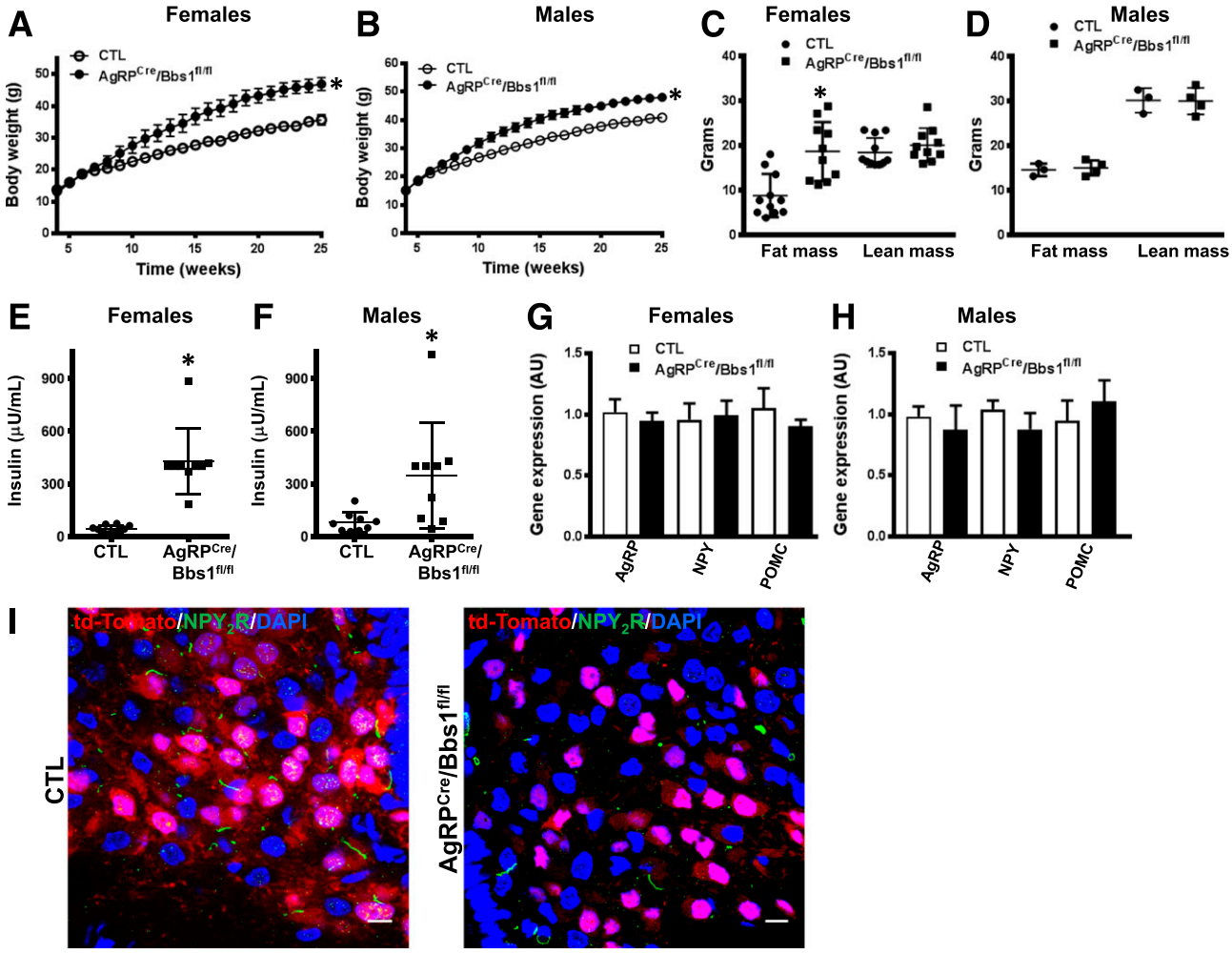

Figure 2—*Bbs1* gene deletion in AgRP neurons causes obesity. Weekly body weights of female (*A*) and male (*B*) mice (n = 10–23/group: 19 males and 23 females for controls [CTL] and 15 males and 10 females for AgRP^{cre}/Bbs1$^{fl/fl}$ mice). *C* and *D*: Fat and lean masses. *E* and *F*: Plasma insulin levels. *G* and *H*: Hypothalamic mRNA levels of metabolic neuropeptides (n = 6/group). *I*: Selective loss of ciliary localization of NPY$_2$R in td-Tomato$^+$ neurons of the hypothalamic arcuate nucleus of AgRP^{cre}/Bbs1$^{fl/fl}$ mice. *$P < 0.05$ vs. control group. Scale bars, 10 μm.

Surprisingly and in contrast to our expectation, mice lacking expression of the *Bbs1* gene in AgRP neurons (AgRP^{Cre}/Bbs1$^{fl/fl}$) developed obesity, as indicated by the significantly increased body weight, starting at ∼6 weeks of age (Fig. 2*A* and *B*). Notably, this increase in body weight was more pronounced in the females relative to the males, suggesting that loss of the BBSome in AgRP neurons may contribute to the sex difference in the development of obesity in BBS mice (24,25). Fat mass was increased in female but not male AgRP^{cre}/Bbs1$^{fl/fl}$ mice (Fig. 2*C* and *D* and Supplementary Fig. 3*B* and *C*) without alteration in lean mass (Fig. 2*C* and *D*). Consistent with body weight, the increase in liver mass was more noticeable in female than in male AgRP^{cre}/Bbs1$^{fl/fl}$ mice (females: 2.74 ± 0.46 vs. 1.58 ± 0.12 g, $P < 0.05$; males: 3.41 ± 0.58 vs. 2.45 ± 0.22 g, P = 0.06). Of note, plasma insulin levels were elevated in female and male AgRP^{cre}/Bbs1$^{fl/fl}$ mice relative to control littermates (Fig. 3*E* and *F*).

There was no significant change in the expression of hypothalamic anorexigenic and orexigenic genes in AgRP^{cre}/Bbs1$^{fl/fl}$ mice compared with control littermates, although expression of AgRP tended to be lower in AgRP^{cre}/Bbs1$^{fl/fl}$ mice (Fig. 2*G*). These findings indicate that different molecular mechanisms may underlie the obesity phenotype of AgRP^{cre}/Bbs1$^{fl/fl}$ mice versus POMC^{cre}/Bbs1$^{fl/fl}$ mice.

Consistent with the previous report (17), localization of NPY$_2$R in primary cilia of td-Tomato$^+$ cells was substantially reduced in AgRP^{cre}/Bbs1$^{fl/fl}$ mice (Fig. 2*H*). Of note, there was no difference in *Npy2r* gene expression between AgRP^{cre}/Bbs1$^{fl/fl}$ mice (1.4 ± 0.4 arbitrary units [AU]) and controls (1.0 ± 0.3 AU). These findings confirm the importance of the BBSome for the trafficking of key metabolic receptors in hypothalamic neurons.

Plasma Membrane Localization of 5-HT$_{2C}$R in POMC Neurons Required the BBSome

Next, we asked whether the BBSome is involved in the trafficking of other receptors that are important for energy homeostasis, such as the serotonin 5-HT$_{2C}$R, which is

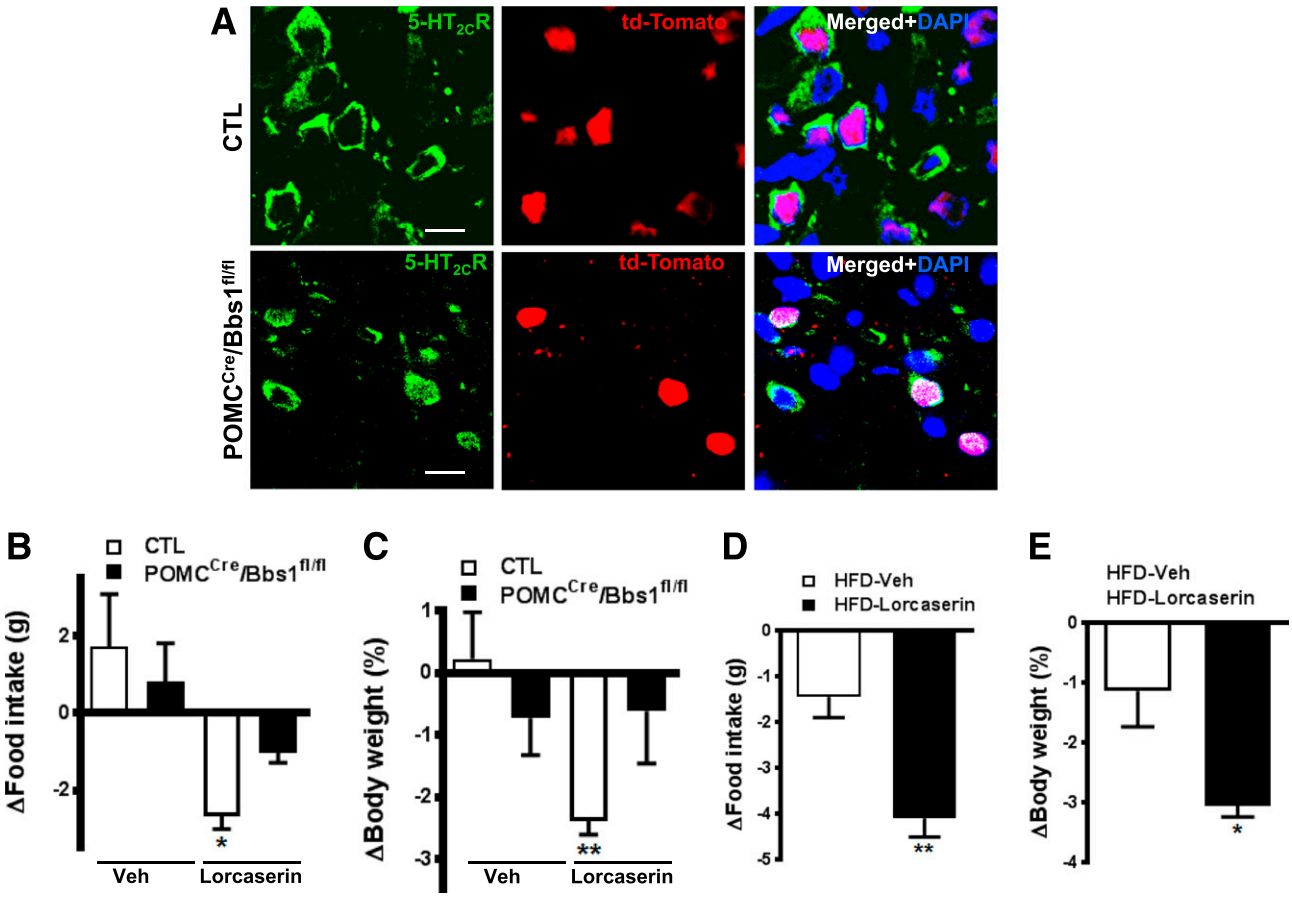

Figure 3—The BBSome mediates surface expression of the 5-HT$_{2C}$R in POMC neurons. *A*: Reduced membrane localization of the 5-HT$_{2C}$R in td-Tomato$^+$ cells of POMC^{Cre}/Bbs1$^{fl/fl}$ mice. *B* and *C*: Blunted lorcaserin-induced decrease in food intake and body weight in POMC^{Cre}/Bbs1$^{fl/fl}$ mice. CTL, control; Veh, vehicle. Lorcaserin decreases food intake (*D*) and body weight (*E*) in high-fat diet (HFD)–induced obese mice. *$P < 0.05$ and **$P < 0.01$ vs. control group. Scale bars, 10 μm.

present in POMC neurons (7,26). Using an antibody that recognizes specifically the 5-HT$_{2C}$R, as confirmed by Western blot and immunohistochemistry in cells and arcuate nucleus of *5-HT$_{2C}$R$^{-/-}$* null mice (Supplementary Fig. 4*A*–*C*), we found that in the arcuate nucleus of control mice, 5-HT$_{2C}$R is predominantly present in the plasma membrane of td-Tomato$^+$ cells as well as in some td-Tomato$^-$ cells (Fig. 3*A*). Notably, in POMC^{cre}/Bbs1$^{fl/fl}$ mice, the localization of 5-HT$_{2C}$R is altered selectively in td-Tomato$^+$ cells, appearing stalled in the cytoplasm (Fig. 3*A*). Of note, 5-HT$_{2C}$R does not localize in cilia of td-Tomato$^+$ or td-Tomato$^-$ cells of the hypothalamic arcuate nucleus of control and POMC^{cre}/Bbs1$^{fl/fl}$ mice. In contrast, the NPY$_2$R localizes predominantly in neuronal cilia, and POMC^{cre}/Bbs1$^{fl/fl}$ mice displayed reduced ciliary localization of this receptor in td-Tomato$^+$ cells of the arcuate nucleus (Supplementary Fig. 5*A* and *B*). Hypothalamic mRNA levels of 5-HT$_{2C}$R and NPY$_2$R were not altered in POMC^{cre}/Bbs1$^{fl/fl}$ mice (0.9 ± 0.1 and 1.2 ± 0.3 AU, respectively) relative to littermate controls (1.0 ± 0.1 AU for both). AgRP^{cre}/Bbs1$^{fl/fl}$ mice also exhibit normal hypothalamic mRNA levels of 5-HT$_{2C}$R (0.9 ± 0.1 AU) compared to controls (1.0 ± 0.2 AU). Interestingly, deletion of the *Bbs1* gene does not appear to affect cilia formation, as indicated by the relatively normal cilia, stained with adenylyl cyclase type III, in the arcuate nucleus td-Tomato$^+$ cells of POMC^{cre}/Bbs1$^{fl/fl}$ mice (Supplementary Fig. 5*B*).

Based on the evidence above, we predicted that the metabolic effects evoked by activation of 5-HT$_{2C}$R would be blunted in POMC^{cre}/Bbs1$^{fl/fl}$ mice. Thus, we assessed the anorectic and weight-reducing responses induced by the 5-HT$_{2C}$R agonist, lorcaserin. In control mice, lorcaserin decreases food intake and body weight (Fig. 3*B* and *C*). However, the responses evoked by lorcaserin are significantly blunted in POMC^{cre}/Bbs1$^{fl/fl}$ mice. The reduced responses to lorcaserin in POMC^{cre}/Bbs1$^{fl/fl}$ mice does not appear due to obesity but rather caused by loss of the BBSome. This is supported by the decrease in food intake and body weight in diet-induced obese mice treated with lorcaserin (Fig. 3*D* and *E*). Taken together, these data demonstrate the importance of the BBSome in POMC neurons in underlying serotonin-mediated control of energy homeostasis.

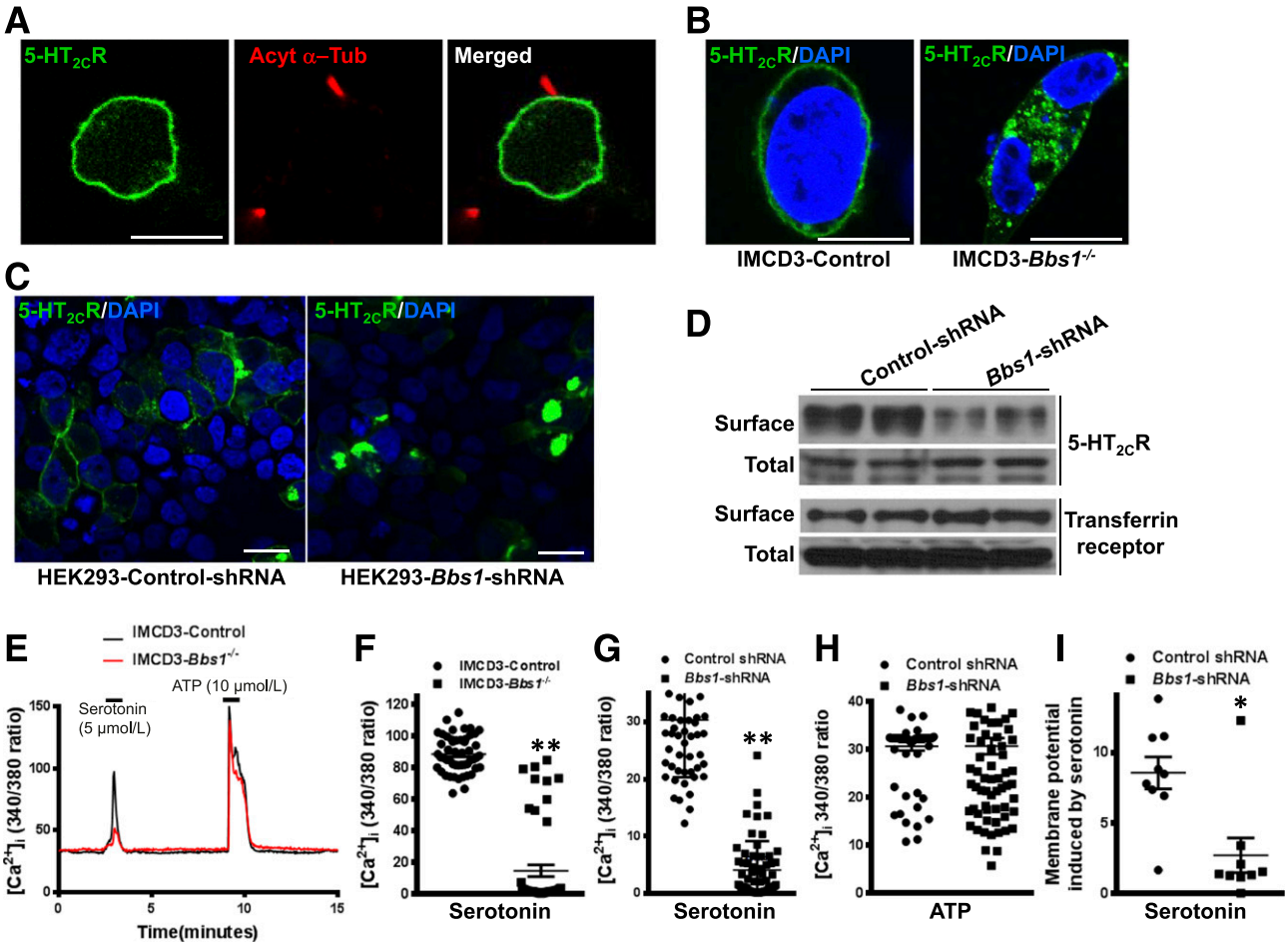

Figure 4— The BBSome is required for the cellular responses evoked by the 5-HT_{2C}R. *A*: Lack of localization of 5-HT_{2C}R in cilia (labeled with acetylated α-tubulin [Acyt α-Tub]) in IMCD3 cells. *B*: Reduced membrane localization of 5-HT_{2C}R in IMCD3-*Bbs1*$^{-/-}$ cells. *Bbs1* gene silencing reduces the surface levels of 5-HT_{2C}R, but not transferrin receptor, in HEK 293 cells by immunostaining and biotin labeling assay (*C*), followed by Western blotting (*D*). *E* and *F*: Reduced $[Ca^{2+}]$i response to serotonin in IMCD3-*Bbs1*$^{-/-}$ cells. *Bbs1* gene silencing decreases $[Ca^{2+}]$i response to serotonin (*G*), but not ATP (*H*), and reduces the membrane potential evoked by serotonin (*I*) in HEK 293 cells. $^{*}P < 0.01$ and $^{**}P < 0.0001$ vs. control group. Scale bars, 10 μm.

BBSome Deficiency Hinders Serotonin-Evoked Cellular Responses

To facilitate the analysis of the trafficking of the 5-HT_{2C}R in vitro, we generated a GFP-tagged receptor (5-HT_{2C}R–GFP). First, we used confocal microscopy to investigate the membrane localization of the 5-HT_{2C}R in the IMCD3 cell line. Although 5-HT_{2C}R–GFP was present in the plasma membrane, we were unable to detect 5-HT_{2C}R–GFP in cilia (labeled with acetylated α-tubulin) (Fig. 4*A*), indicating that the 5-HT_{2C}R is not targeted to the cilium. In contrast, we found that NPY_2R and $SSTR_3$ localize almost exclusively to cilia in IMCD3 cells (Supplementary Fig. 6*A* and *B*).

Next, we tested whether loss of the BBSome interferes with the membrane localization of 5-HT_{2C}R in IMCD3 cells. Interestingly, *Bbs1* gene disruption using CRISPR/Cas9 reduced 5-HT_{2C}R–GFP in the plasma membrane (Fig. 4*B*), confirming the importance of the BBSome for membrane localization of the 5-HT_{2C}R. In addition, the NPY_2R and $SSTR_3$ both failed to localize to cilia in IMCD3-*Bbs1*$^{-/-}$ cells (Supplementary Fig. 6*A* and *B*), confirming the importance of the BBSome for the trafficking of these receptors to cilia. Consistent with the observation in POMC neurons, the 5-HT_{2C}R in the IMCD3-*Bbs1*$^{-/-}$ cells was predominantly localized in unusual large cytoplasmic vesicles (Fig. 4*B*).

Like CRISPR/Cas9-mediated deletion in IMCD3 cells, shRNA-induced silencing of *Bbs1* gene expression reduces the membrane localization of 5-HT_{2C}R in HEK 293 cells (Fig. 4*C*). Most of the GFP-tagged 5-HT_{2C}R localizes to the plasma membrane in the control cells (transfected with scrambled shRNA), whereas the localization of this receptor is mostly in vesicles in the *Bbs1*-shRNA–transfected HEK 293 cells. The reduced amount of 5-HT_{2C}R in the plasma membrane of HEK 293 cells transfected with *Bbs1*-shRNA was further confirmed using a cell surface biotin labeling assay, followed by Western blotting (Fig. 4*D*). Importantly, total 5-HT_{2C}R expression is not changed when the *Bbs1* gene is silenced. In addition, the surface level of the transferrin receptor is not affected by *Bbs1* gene silencing (Fig. 4*D*), demonstrating the specificity of

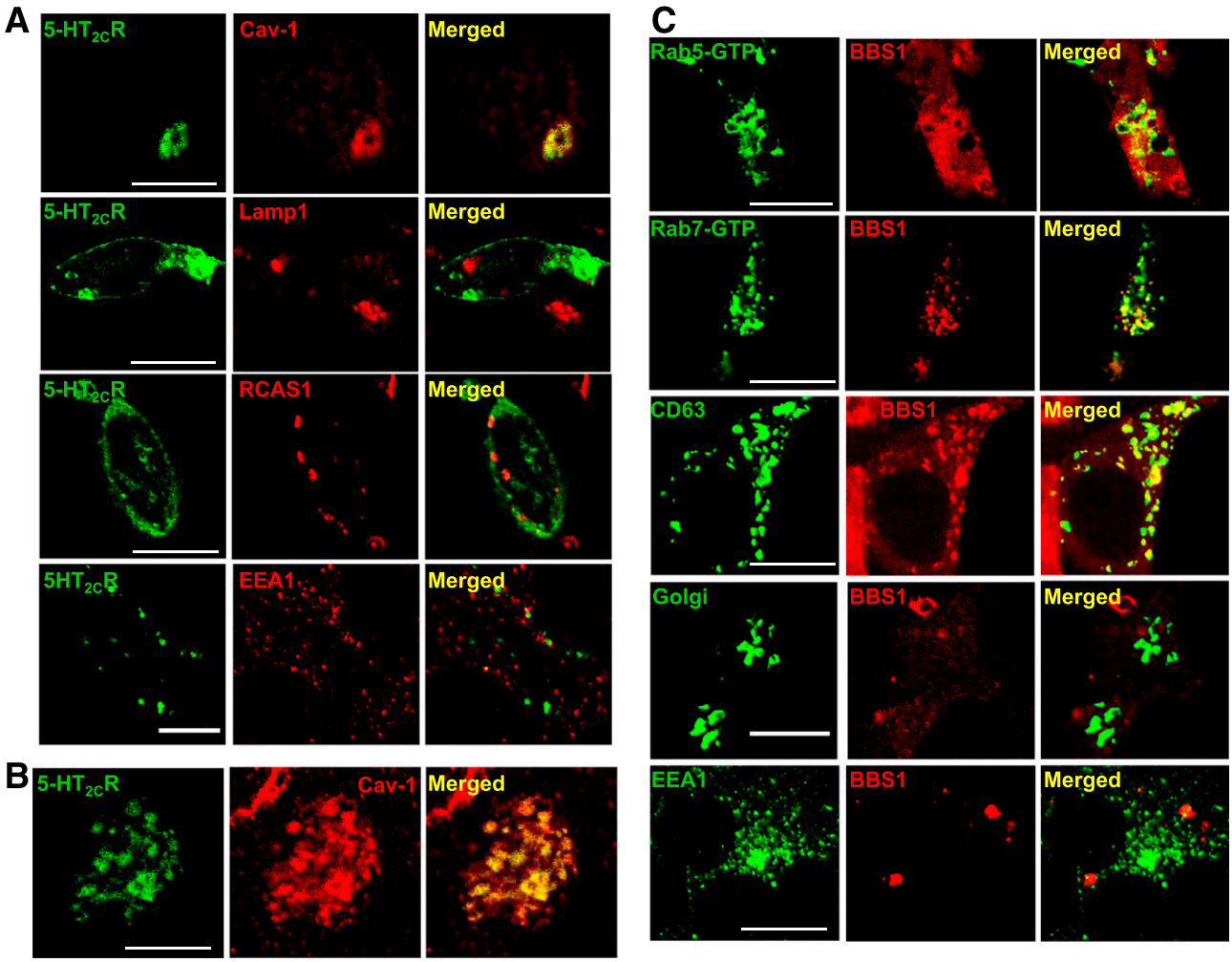

Figure 5—Localization of 5-HT_{2C}R and BBS1 in the secretory pathway. *A*: GFP-tagged 5-HT_{2C}R localizes in the endosome (Cav-1) but not in the lysosome (LAMP1), Golgi (RSAC1), or early endosome (EEA1) in IMCD3-*Bbs1*$^{-/-}$ cells. *B*: Colocalization of 5-HT_{2C}R–GFP and Cav-1 is only partial when the expression of 5-HT_{2C}R–GFP is high. *C*: RFP-tagged BBS1 colocalizes with GFP-tagged Rab5-GTP, Rab7-GTP, and CD63 (markers of the late endosome) but not with markers of Golgi or early endosome (EEA1) in HEK 293 cells. Scale bars, 10 μm.

the effects evoked by BBS1 loss on receptor trafficking to the plasma membrane.

We studied the functional consequence of altered 5-HT_{2C}R trafficking in the absence of the BBSome by assessing the response of $[Ca^{2+}]$i to serotonin. Compared with control cells, the serotonin-induced increase in $[Ca^{2+}]$i is substantially decreased in IMCD3-*Bbs1*$^{-/-}$ cells (Fig. 4*E* and *F*) and HEK 293 cells transfected with *Bbs1*-shRNA (Fig. 4*G*). The leptin-evoked increase in $[Ca^{2+}]$i is also blunted after BBSome disruption (Supplementary Fig. 7). However, the increase in $[Ca^{2+}]$i evoked by ATP was not altered by disruption of the BBSome (Fig. 4*E* and *H*). We also examined the effects of silencing the *Bbs1* gene on serotonin-induced membrane potential using patch-clamp recording. Membrane potential response to serotonin is dramatically reduced in HEK 293 cells transfected with *Bbs1*-shRNA compared with control cells (Fig. 4*I*). These results demonstrate that reduction in 5-HT_{2C}R trafficking to the plasma membrane caused by disruption of the BBSome is associated with attenuated cellular responses evoked by serotonin.

Stalled 5-HT_{2C}R in the Late Endosome in the Absence of the BBSome

The reduced membrane localization of the 5-HT_{2C}R without alteration in its total expression when the BBSome is disrupted indicates that the receptor is stuck in the secretory pathway. To understand the fate of 5-HT_{2C}R in cells lacking the *Bbs1* gene, we first studied the localization of the receptor in the secretory pathway using markers of key organelles, including caveolin-1 (Cav-1) (endosome), LAMP1 (lysosome), RSAC1 (Golgi), and EEA1 (early endosome) using IMCD3-*Bbs1*$^{-/-}$ cells. Interestingly, we observed that 5-HT_{2C}R–GFP colocalizes predominantly with the endosome marker, Cav-1, when 5-HT_{2C}R–GFP expression is low (Fig. 5*A*). This localization of 5-HT_{2C}R–GFP and Cav-1 is only partial when the expression of 5-HT_{2C}R–GFP is high (Fig. 5*B*).

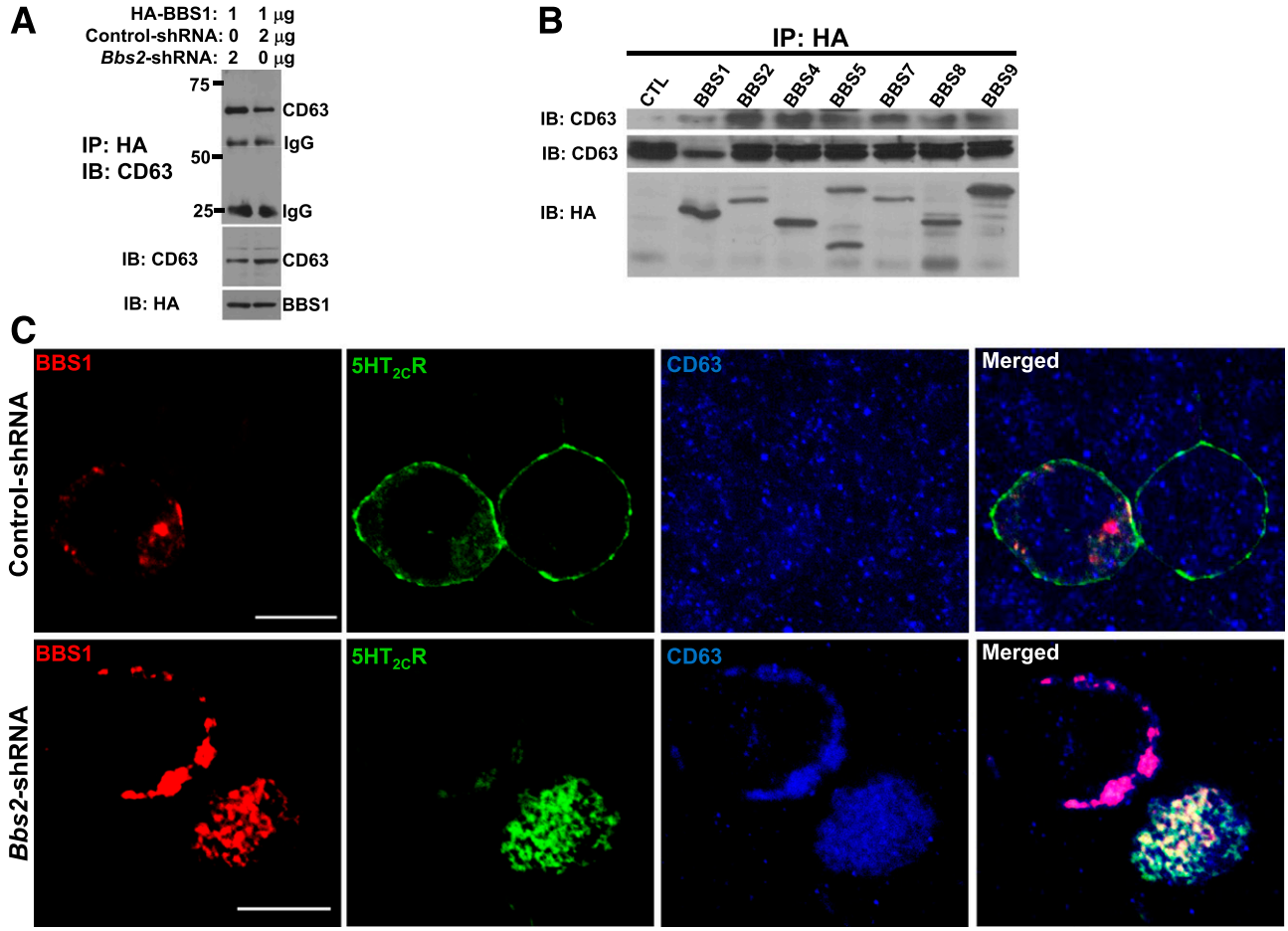

Figure 6—BBSome proteins interact with CD63. *A*: Coimmunoprecipitation of the HA-tagged BBS1 with the endogenous CD63 (late endosome marker) is enhanced after *Bbs2* gene silencing in HEK 293 cells. *B*: BBSome proteins interact with CD63 in a coimmunoprecipitation assay. *C*: *Bbs2* gene silencing promotes localization of BBS1 with 5-HT_{2C}R in the late endosome. Scale bars, 10 μm. IB, immunoblot; IP, immunoprecipitation.

We next analyzed the cellular localization of BBS proteins. For this, HEK 293 cells were transiently cotransfected with RFP-BBS1 along with GFP-tagged marker proteins of early endosome (Rab5 constitutive active form, Rab5–guanosine-5'-triphosphate [GTP]), late endosome (Rab7 constitutive active form Rab7-GTP or CD63), Golgi or early endosome (EEA1), and localization was visualized with confocal microscopy. We found that RFP-BBS1 colocalized with the late endosome marker proteins, Rab7-GTP and CD63, and partially colocalized with Rab5-GTP but not with Golgi or early endosome markers (Fig. 5*C*). Similarly, RFP-BBS7 colocalized with the late endosome proteins Rab7-GTP and CD63 (Supplementary Fig. 8*A*).

To test whether the BBSome proteins physically interact with CD63, HEK 293 cells were transiently transfected with HA-tagged BBS1 protein. BBS1 protein was then immunoprecipitated with HA-agarose beads, and the endogenous CD63 protein was detected with CD63 antibody by Western blot. As shown in Fig. 6*A*, CD63 protein is detected in a BBS-immunoprecipitated protein complex. Furthermore, silencing *BBS2* increased BBS1 interaction with the CD63 compared with control shRNA (Fig. 6*A*), indicating the specificity of their interaction. We then tested whether other subunits of the BBSome also interact with the CD63 in HEK 293 cells. We found that in addition to BBS1, other BBSome proteins, including BBS2, BBS4, BBS5, BBS7, BBS8, and BBS9, interact with the endogenous CD63 (Fig. 6*B*). On one hand, in HEK 293 cells overexpressing BBS1 or BBS7 proteins, endogenous CD63 protein colocalizes with BBS1 or BBS7, whereas 5-HT_{2C}R is mostly present in the plasma membrane (Fig. 6*C* and Supplementary Fig. 8*B*). On the other hand, disruption of the BBSome by silencing *BBS2* in HEK 293 cells causes 5-HT_{2C}R to colocalize with BBS1 or BBS7 with the endogenous CD63 protein. In contrast, 5-HT_{2C}R appears in the plasma membrane when the BBSome complex is intact (Fig. 6*C* and Supplementary Fig. 8*B*). These results indicate that loss of the BBSome causes 5-HT_{2C}R to stall in the late endosome, possibly forming a complex with CD63 and the remaining BBS proteins.

DISCUSSION

There are several new findings in the current study. First, we show that targeted disruption of the BBSome by

deleting the *Bbs1* gene in POMC neurons leads to obesity. We demonstrate that obesity in these mice is associated with an increase in food intake. Second, we provide evidence that mice lacking the BBSome in AgRP neurons also display an increase in body weight and fat mass. Third, we identify an important role for the BBSome in mediating the trafficking of the 5-HT_{2C}R in POMC neurons. We demonstrate that loss of the BBSome reduces surface expression of the 5-HT_{2C}R and interferes with the ability of serotonin to modulate cellular processes. In absence of the BBSome, 5-HT_{2C}R becomes stalled in the late endosome of the secretory pathway. Together, these findings provide mechanistic insights into the contribution of the hypothalamic BBSome to the control of energy balance and handling of metabolic receptors.

Substantial evidence points to the importance of POMC and AgRP neurons as first-order neurons in the neurocircuit that controls metabolic functions (3,6). These neurons are equipped with receptors for various metabolic signals, including serotonin, and regulate the downstream neurocircuitry to enact appropriate and consequential metabolic and behavioral responses to maintain energy balance. Several cellular processes within POMC and/or AgRP neurons have previously been shown to have important implications for metabolic control. This includes gene expression (22), protein translation and processing (27,28), endoplasmic reticulum stress (29,30), and mitochondria function (31–34). The changes in the trafficking of metabolic receptors evoked by disruption of the BBSome in POMC and AgRP neurons extend the cellular processes within these neurons that influence energy homeostasis.

We demonstrate that absence of the BBSome substantially reduces surface expression of the 5-HT_{2C}R in cultured cells and POMC neurons. In BBSome-deficient cells the 5-HT_{2C}R is held up in large vesicles in the cytoplasm. We previously demonstrated that the LepRb is also stalled in large cellular vesicles when the BBSome is disrupted (23). To determine the identity of these vesicles, we analyzed the localization of the BBSome proteins and 5-HT_{2C}R in key organelles of the secretary pathway. We found that BBS proteins colocalize with the late endosome markers and partially colocalize with the early endosome marker. Importantly, we have identified the late endosome as the vesicle where the 5-HT_{2C}R is held up when the BBSome is disrupted. Future studies will determine what makes the receptors stall in this stage of the secretory pathway after loss of the BBSome. Additional studies are also needed to assess the possibility of overcoming the mistrafficking of metabolic receptors when the BBSome is disrupted.

Obesity is a major phenotype criterion in patients with BBS (15,35). Mice carrying deletion or mutations in *BBS* genes also display an obesity phenotype that is driven by hyperphagia and a decrease in energy expenditure (23,36). These findings point to a fundamental role of BBS proteins in the regulation of appetite and energy balance. This has triggered tremendous interest in understanding the mechanisms underlying the control of energy homeostasis by the BBSome. We previously demonstrated that loss of the BBSome in the nervous system or LepRb-containing cells, but not in adipocytes, largely recapitulated the increase in body weight and food intake associated with BBS (20). Our findings that BBSome deficiency in POMC neurons or AgRP neurons is sufficient to increase body weight and adiposity demonstrate the importance of the BBSome in these neuronal populations. The decreased hypothalamic POMC mRNA levels in mice lacking the *BBS* gene globally or in defined neuronal populations, such as POMC neurons, is consistent with the defective signaling of receptors that regulate *Pomc* gene expression, including LepRb and NPY_2R (37,38). This reduction in *Pomc* gene expression may contribute to the hyperphagia and obesity associated with BBS. Thus, the obesity associated with BBS may emanate from loss of the BBSome in hypothalamic neurons.

We also speculate that our findings may have implications for understanding the abnormalities associated with common obesity. This is supported by the demonstration that variants of *BBS* genes increase susceptibility to common human obesity (12–14). Of note, a reduction in surface expression of hypothalamic receptors was reported in animals with dietary obesity (39). A possible contribution of the BBSome to the abnormalities associated with common obesity warrants further investigation.

One limitation of our study relates to the use of mice expressing constitutive $POMC^{Cre}$ and $AgRP^{Cre}$ to delete the *Bbs1* gene in these neuronal populations since embryonic expression of Cre may have deleted the *Bbs1* gene in peripheral tissues and cells that do not necessarily differentiate to POMC or AgRP neurons. Indeed, a subset of POMC-expressing progenitor cells are known to differentiate to other cell types, including AgRP neurons (40), which can result in misleading feeding responses when constitutive $POMC^{Cre}$ mice are used (41). It should be noted, however, that constitutive $POMC^{Cre}$ and $AgRP^{Cre}$ were used successfully to dissociate the contribution of POMC versus AgRP neurons to leptin regulation of regional autonomic nerve activity (21). Nonetheless, the recent development of inducible $POMC^{Cre}$ (26) and $AgRP^{Cre}$ mice (42) that allow circumventing the issues related to constitutive Cre activation will be useful to test the effects of *Bbs1* gene deletion in POMC and AgRP neurons of adult mice.

The use of in vitro systems, including a kidney cell line (HEK 293), to understand the neuronal mechanisms of obesity in our conditional mouse models can also be viewed as a limitation to our studies. However, in vitro studies are very useful to examine the biology of the BBSome and gain mechanistic insights into its function. Importantly, we provide evidence showing that the in vitro data are recapitulated in vivo, as indicated by the similar defects in the trafficking of NPY_2R and 5-HT_{2C}R evoked by loss of the BBSome in cultured cells and hypothalamic neurons.

In conclusion, our findings point to the BBSome in POMC and AgRP neurons as a critical regulator of energy homeostasis. Our results enhance our understanding of the cellular and molecular processes that underlie obesity in BBS with potential implications for common obesity.

Funding. This work was supported by funds from the National Institutes of Health (grant NS-096246 to Y.M.U., HL-134850 to J.L.G., EY-011298 to V.C.S., and HL-084207 to K.R.), the American Heart Association (18EIA33890055 to J.L.G. and 14EIA18860041 to K.R.), and the University of Iowa Fraternal Order of Eagles Diabetes Research Center to K.R. The Zeiss LSM710 in the University of Iowa's Central Microscopy Research Facilities used for confocal imaging is funded by the National Institutes of Health (grant 1S10-RR-025439-01).

Duality of Interest. No potential conflicts of interest relevant to this article were reported.

Author Contributions. D.-F.G. designed and performed the experiments and wrote the manuscript. Z.L. performed the calcium experiments. Y.W. performed the electrophysiology experiments. C.S. created the knockout cell line. D.R.T. measured body composition by MRI. G.B.R., Y.M.U., J.L.G., and V.C.S. helped with experimental design and data interpretation. J.L.G. measured energy expenditure. K.R. conceptualized, analyzed, and interpreted studies and wrote the manuscript. K.R. is the guarantor of this work and, as such, had full access to all the data in the study and takes responsibility for the integrity of the data and the accuracy of the data analysis.

References

1. Willer CJ, Speliotes EK, Loos RJF, et al.; Wellcome Trust Case Control Consortium; Genetic Investigation of ANthropometric Traits Consortium. Six new loci associated with body mass index highlight a neuronal influence on body weight regulation. Nat Genet 2009;41:25–34

2. Locke AE, Kahali B, Berndt SI, et al.; LifeLines Cohort Study; ADIPOGen Consortium; AGEN-BMI Working Group; CARDIOGRAMplusC4D Consortium; CKDGen Consortium; GLGC; ICBP; MAGIC Investigators; MuTHER Consortium; MIGen Consortium; PAGE Consortium; ReproGen Consortium; GENIE Consortium; International Endogene Consortium. Genetic studies of body mass index yield new insights for obesity biology. Nature 2015;518:197–206

3. Morton GJ, Cummings DE, Baskin DG, Barsh GS, Schwartz MW. Central nervous system control of food intake and body weight. Nature 2006;443:289–295

4. Elmquist JK, Elias CF, Saper CB. From lesions to leptin: hypothalamic control of food intake and body weight. Neuron 1999;22:221–232

5. Cui H, López M, Rahmouni K. The cellular and molecular bases of leptin and ghrelin resistance in obesity. Nat Rev Endocrinol 2017;13:338–351

6. Andermann ML, Lowell BB. Toward a wiring diagram understanding of appetite control. Neuron 2017;95:757–778

7. Wyler SC, Lord CC, Lee S, Elmquist JK, Liu C. Serotonergic control of metabolic homeostasis. Front Cell Neurosci 2017;11:277

8. Nachury MV, Loktev AV, Zhang Q, et al. A core complex of BBS proteins cooperates with the GTPase Rab8 to promote ciliary membrane biogenesis. Cell 2007;129:1201–1213

9. Loktev AV, Zhang Q, Beck JS, et al. A BBSome subunit links ciliogenesis, microtubule stability, and acetylation. Dev Cell 2008;15:854–865

10. Seo S, Baye LM, Schulz NP, et al. BBS6, BBS10, and BBS12 form a complex with CCT/TRiC family chaperonins and mediate BBSome assembly. Proc Natl Acad Sci U S A 2010;107:1488–1493

11. Zhang Q, Yu D, Seo S, Stone EM, Sheffield VC. Intrinsic protein-protein interaction-mediated and chaperonin-assisted sequential assembly of stable Bardet-Biedl syndrome protein complex, the BBSome. J Biol Chem 2012;287:20625–20635

12. Benzinou M, Walley A, Lobbens S, et al. Bardet-Biedl syndrome gene variants are associated with both childhood and adult common obesity in French Caucasians. Diabetes 2006;55:2876–2882

13. Lim ET, Liu YP, Chan Y, et al.; Go-T2D Consortium. A novel test for recessive contributions to complex diseases implicates Bardet-Biedl syndrome gene BBS10 in idiopathic type 2 diabetes and obesity. Am J Hum Genet 2014;95:509–520

14. Hendricks AE, Bochukova EG, Marenne G, et al.; Understanding Society Scientific Group; EPIC-CVD Consortium; UK10K Consortium. Rare variant analysis of human and rodent obesity genes in individuals with severe childhood obesity. Sci Rep 2017;7:4394

15. Guo DF, Rahmouni K. Molecular basis of the obesity associated with Bardet-Biedl syndrome. Trends Endocrinol Metab 2011;22:286–293

16. Jin H, White SR, Shida T, et al. The conserved Bardet-Biedl syndrome proteins assemble a coat that traffics membrane proteins to cilia. Cell 2010;141:1208–1219

17. Loktev AV, Jackson PK. Neuropeptide Y family receptors traffic via the Bardet-Biedl syndrome pathway to signal in neuronal primary cilia. Cell Rep 2013;5:1316–1329

18. Siljee JE, Wang Y, Bernard AA, et al. Subcellular localization of MC4R with ADCY3 at neuronal primary cilia underlies a common pathway for genetic predisposition to obesity. Nat Genet 2018;50:180–185

19. Starks RD, Beyer AM, Guo DF, et al. Regulation of insulin receptor trafficking by Bardet Biedl syndrome proteins. PLoS Genet 2015;11:e1005311

20. Guo DF, Cui H, Zhang Q, et al. The BBSome controls energy homeostasis by mediating the transport of the leptin receptor to the plasma membrane. PLoS Genet 2016;12:e1005890

21. Bell BB, Harlan SM, Morgan DA, Guo DF, Cui H, Rahmouni K. Differential contribution of POMC and AgRP neurons to the regulation of regional autonomic nerve activity by leptin [published correction appears in Mol Metab 2018;14:158]. Mol Metab 2018;8:1–12

22. Henry FE, Sugino K, Tozer A, Branco T, Sternson SM. Cell type-specific transcriptomics of hypothalamic energy-sensing neuron responses to weight-loss. eLife 2015;4:e09800

23. Seo S, Guo DF, Bugge K, Morgan DA, Rahmouni K, Sheffield VC. Requirement of Bardet-Biedl syndrome proteins for leptin receptor signaling. Hum Mol Genet 2009;18:1323–1331

24. Fath MA, Mullins RF, Searby C, et al. Mkks-null mice have a phenotype resembling Bardet-Biedl syndrome. Hum Mol Genet 2005;14:1109–1118

25. Davis RE, Swiderski RE, Rahmouni K, et al. A knockin mouse model of the Bardet-Biedl syndrome 1 M390R mutation has cilia defects, ventriculomegaly, retinopathy, and obesity. Proc Natl Acad Sci U S A 2007;104:19422–19427

26. Berglund ED, Liu C, Sohn JW, et al. Serotonin 2C receptors in pro-opiomelanocortin neurons regulate energy and glucose homeostasis [published correction appears in J Clin Invest 2014;124:1868]. J Clin Invest 2013;123:5061–5070

27. Creemers JW, Pritchard LE, Gyte A, et al. Agouti-related protein is post-translationally cleaved by proprotein convertase 1 to generate agouti-related protein (AGRP)83-132: interaction between AGRP83-132 and melanocortin receptors cannot be influenced by syndecan-3. Endocrinology 2006;147:1621–1631

28. Yasuda A, Jones LS, Shigeri Y. The multiplicity of post-translational modifications in pro-opiomelanocortin-derived peptides. Front Endocrinol (Lausanne) 2013;4:186

29. Zhang X, Zhang G, Zhang H, Karin M, Bai H, Cai D. Hypothalamic IKKbeta/NF-kappaB and ER stress link overnutrition to energy imbalance and obesity. Cell 2008;135:61–73

30. Williams KW, Liu T, Kong X, et al. Xbp1s in Pomc neurons connects ER stress with energy balance and glucose homeostasis. Cell Metab 2014;20:471–482

31. Dietrich MO, Liu ZW, Horvath TL. Mitochondrial dynamics controlled by mitofusins regulate Agrp neuronal activity and diet-induced obesity. Cell 2013;155:188–199

32. Schneeberger M, Dietrich MO, Sebastián D, et al. Mitofusin 2 in POMC neurons connects ER stress with leptin resistance and energy imbalance. Cell 2013;155:172–187

33. Santoro A, Campolo M, Liu C, et al. DRP1 suppresses leptin and glucose sensing of POMC neurons. Cell Metab 2017;25:647–660
34. Ramírez S, Gómez-Valadés AG, Schneeberger M, et al. Mitochondrial dynamics mediated by mitofusin 1 is required for POMC neuron glucose-sensing and insulin release control. Cell Metab 2017;25:1390–1399.e6
35. Mujahid S, Hunt KF, Cheah YS, et al. The endocrine and metabolic characteristics of a large Bardet-Biedl syndrome clinic population. J Clin Endocrinol Metab 2018;103:1834–1841
36. Rahmouni K, Fath MA, Seo S, et al. Leptin resistance contributes to obesity and hypertension in mouse models of Bardet-Biedl syndrome. J Clin Invest 2008; 118:1458–1467
37. Schwartz MW, Seeley RJ, Woods SC, et al. Leptin increases hypothalamic pro-opiomelanocortin mRNA expression in the rostral arcuate nucleus. Diabetes 1997;46:2119–2123
38. Sainsbury A, Schwarzer C, Couzens M, et al. Important role of hypothalamic Y2 receptors in body weight regulation revealed in conditional knockout mice. Proc Natl Acad Sci U S A 2002;99:8938–8943
39. Irani BG, Dunn-Meynell AA, Levin BE. Altered hypothalamic leptin, insulin, and melanocortin binding associated with moderate-fat diet and predisposition to obesity. Endocrinology 2007;148:310–316
40. Padilla SL, Carmody JS, Zeltser LM. Pomc-expressing progenitors give rise to antagonistic neuronal populations in hypothalamic feeding circuits. Nat Med 2010;16:403–405
41. Wei Q, Krolewski DM, Moore S, et al. Uneven balance of power between hypothalamic peptidergic neurons in the control of feeding. Proc Natl Acad Sci U S A 2018;115:E9489–E9498
42. Wang Q, Liu C, Uchida A, et al. Arcuate AgRP neurons mediate orexigenic and glucoregulatory actions of ghrelin. Mol Metab 2013;3:64–72